Version of Record: https://www.sciencedirect.com/science/a1ticle/pii/S0165237024002559
Manuscript a00a89ddec1ff53588540eeb21c36706

Role of sodium sulfate in electrical conductivity and structure of lignin-derived carbons

Seth Kane[a]*, David B. Hodge[b] , Brian Saulnier[b] , Vi116 Enik6 Bécsy-Jakab[b], Dilara N. Dülger[b] , Cecily Ryan[a]

[a]Montana State University, Bozeman, MT 59717, United States, Mechanical and Industrial Engineering [b] Montana State University, Bozeman, MT 59717, United States, Chemical and Biological Engineermg

Abstract

Lignin is a promising renewable alternative to fossil fuels for producing carbon materials such as carbon fibers, activated carbons, or carbon black. Despite extensive research, lignin-derived carbon materials show limited graphitization relative to comparable petroleum-derived carbons. Further, ligninderived carbons show high variation in graphitization and electrical conductivity depending on the source of the lignin. Herein, nine lignins, derived from various feedstocks and isolation procedures, are pyrolyzed to produce biochar at 1100 ^{0} C. These lignins have a range of chemical compositions, carbon structures, and particle sizes. As a result, the pyrolysis behavior of these lignins varies, with powdered, clumped powder, and "foam" biochar morphologies resulting from finely powdered lignin. The produced biochars vary widely

*Corresponding author, sethkane@montana.edu, (907)750-6364.
Current address: skane@ucdavis.edu, University of California - Davis, Civil and Environmental Engineering, 2001 Ghausi Hall Davis, CA 95616, USA

in both electrical conductivity, from 0.19 to 19 S/cm, and in-plane graphitic crystallite size, from 3.4 to 41.2 Å. A significant decrease in electrical conductivity is identified when Na2S04 is removed from lignin, accompanied by an increase in graphitic crystallite size. Based on this finding, a quadratic relationship between biochar graphitic crystallite aspect ratio and electrical conductivity is proposed that builds on established quasi-percolation models for biochar electrical conductivity.

Keywords: Biochar, biocarbon, pyrolysis, non-graphitizing carbon, graphitzation.

---

1. Introduction

Developing renewable alternatives to petroleum-derived materials is criti cal to reducing our society's reliance on fossil fuels. Of particular interest are carbon materials, such as carbon black, carbon fibers, and artificial graphite, whose application is expected to grow rapidly in the coming decades [1]. Lignin looks to be a promising alternative feedstock to petroleum due to its high aromatic carbon content [2]. Further, 50-100 Mt of lignin are iso lated annually as a byproduct of paper-making and biorefinery industries [3], which is anticipated to grow as cellulosic biorefineries continue to expand in the coming decade [4]. However, economic factors primarily limit upcy cling of lignin waste streams [5]. As carbon materials are considered some of the most valuable products of lignin [6], the development of simple pro cesses to convert this lignin to renewable carbon materials has the potential to both reduce reliance on petroleum products and upcycle this important waste stream.

Lignin-derived carbon materials can be produced via pyrolysis and have been extensively studied [2, 7, 8, 9, 10, 11]. During pyrolysis, oxygen and hydrogen present in lignin react with carbon to form liquid and gas de

composition products, reducing the content of hydrogen and oxygen in the solid phase [12]. The resulting solid material has a graphitic carbon structure, porous morphology, and high electrical conductivity. With optimal processing conditions and feedstock properties, lignin-derived carbons have the potential to replace petroleum-derived materials such as carbon black [11, 13], carbon fibers [7], and activated carbons[14]. Lignin-derived biochars and biocarbons have been examined for a broad set of applications, including electrically conductive plastic additives, replacements for carbon black, and active materials in battery electrodes [11, 13, 15, 16]. Lignin-derived carbons are limited by lower graphitization and increased defects relative to petroleum-derived carbon materials [7, 13, 17, 18]. Further, a large range of electrical conductivity is observed for biochars graphitized at around 1000 ^{0}C, from 0.009 S/cm to 62.96 S/cm for lignins isolated with different processes [10, 19].

These past studies point to lignin as a promising feedstock for various carbon materials; however, its performance is consistently limited by lower graphitization than petroleum-derived carbon materials [7, 13, 17, 18]. Further, wide ranges of electrical conductivity and graphitization have been reported for carbons derived from lignins isolated with different processes. Since graphitization of lignin-derived carbons does not continue to increase above pyrolysis temperatures of approximately 1000 ^{0}C, graphitization cannot typically be increased with higher carbonization temperatures [7, 20, 21].

Lignin molecular weight, inorganic content, and particle size have been identified as critical factors that influence the graphitization of lignin during pyrolysis [7, 10, 15]. Past studies differ in the role that common inorganic compounds, such as sodium sulfate (Na2S04) present in kraft lignins, play in lignin pyrolysis. Some studies have proposed that Na2S04 catalyzes the

formation of graphitic structures, while others propose that Na2S04 inhibits the formation of graphitic structures [22, 23, 24, 25], while recent reviews have highlighted this as an area in need of study [18].

This study investigates the role of different lignin isolation procedures, dominant monomers, parameters, and feedstocks in the graphitization of lignin-derived biochar. Lignins from nine different isolation approaches are characterized for chemical structure, molecular weight, and thermal transitions. These lignins are then pyrolyzed to form biochar at 1100 ^{0}C, and the morphology, chemical composition, carbon structure, and electrical conductivity of these biochar are investigated. First, the relationship between lignin processing and biochar carbon structure is examined. We hypothesize that lignin oxygen content, which is expected to be strongly driven by the ratio of monomers in the lignin, will significantly affect biochar carbon structure and electrical conductivity. Next, the role that Na2S04 plays in lignin pyrolysis is tested directly by removing Na2S04 from lignin. We hypothesize that the presence of Na2S04 in lignin will increase biochar graphitization. This work sheds light on how lignin properties impact carbon structures formed during pyrolysis and can inform feedstock optimization to utilize this important waste stream to create renewable and high-performance carbon materials.

2. Materials and Methods

2.1. Lignin sources and isolation

Three commercial lignins were obtained: alkaline lignin (TCI America, Portland, OR, USA, product # L0082), dealkaline lignin (TCI America, Portland, OR, USA, product # L0045), and alkali lignin (Sigma-Aldrich, Inc., St. Louis, MO, USA, product # 370959). In addition, six laboratory-isolated lignins were produced from hybrid poplar or corn stover using various approaches for lignin isolation and recovery. These lignins vary in feedstock, isolation process, and isolation parameters (Table 1). These processes

are described in detail in the Supplemental Information. After isolation, 75 alkali-corn140, alkali-poplar 150, alkali-poplar 115, and alkali-poplar 145 were 76 washed with deionized water to remove Na2S04, following previously applied 77 procedures [26].

78 Three different treatments were used to reduce lignin particle size prior 79 to pyrolysis to examine the impact of particle size on lignin pyrolysis. The 80 commercial lignins (TCI Alkaline, TCI Dealkaline, and Sigma Alkali) are 81 pyrolyzed as provided. Alkali-poplar 150, alkali-corn140, and alkali-poplar95 82 were ball milled (Retsch Mixer Mill 400) for 3 min at 30 Hz (1800 rpm).

Table 1: Summary of lignin isolation methods and molecular weights (weight average (Mn), number average (Mn), and polydispersity index (PDI)). Listed temperatures are the maximum processing temperatures.

Name (Abbreviation)	Feedstock	Process type	Max. process temp. (°C)	Mw (Da)	Mn (Da)	PDI (Mw/Mn)
TCI Alkaline (TA)	Wood	Commercial, Lignosulfonate	Unk.	60000 [27]	-	-
TCI Dealkaline (TD)	Wood	Commercial, Lignosulfonate	Unk.	60000 [27, 28]	-	-
Sigma Alkali (SA)	Softwood	Commercial, Kraft	Unk.	28000 [28]	5000	5.6
Alkali-corn140 (AC140)	Corn stover	Alkali pretreatment, acidification		11400	3100	3.7
alkali-poplar150 (AP150)	Poplar	Alkali pretreatment, acidification	150	12100		3.4
Alkali-poplar95 (AP95)	Poplar	Alkali pretreatment, acidification	95	8000 [29]	4300	5.3
Hydrolysis-corn (HC)	Corn stover	Alkali pretreatment, enzymatic hydrolysis	150	10000	4100	2.4
Alkali-poplar115 (AP115)	Poplar	[illegible] acidification	115	8700	3500	2.5
Alkali -poplar145 (AP145)	Poplar	Alkali pretreatment, acidification	145	8400	3200	2.7
		Alkali pretreatment, acidification				
		Alkali pretreatment, acidification				

83 Alklai-poplar115, alkali-poplar 145, and hydrolysis-corn were ground with a
84 pestle and mortar for 3 min.

85 2.2. Biochar production

86 All nine lignins were converted to biochar via pyrolysis in a tube furnace. 87 Prior to pyrolysis or analysis, all lignins were stored in a drying oven at 105 88 ° c for at least 24 h to reduce moisture content. Approximately 500 mg of

89 lignin was placed in an alumina boat (100 mm X 20 mm X 13 mm) within 90 the tube furnace (Lindberg/Blue M Mini Mite) fitted with an alumina tube. 91 The tube furnace was purged with nitrogen at 100 mL min ^{I} for 10 min prior 92 to heating. During heating, the purge rate for nitrogen was reduced to 30 93 mL min-I , and the lignin was heated at 10 ^{o} c min-I from room temperature 94 to 1100 ^{0} C, held for 1 h, and then allowed to cool to room temperature. The 95 maximum pyrolysis temperature of 1100 ^{o} c was selected as past studies show 96 limited increases in electrical conductivity at higher pyrolysis temperatures 97 for non-graphitizing feedstocks, such as lignin [21, 30].

98 After pyrolysis, the biochar was ball milled (Retsch Mixer Mill 400 with 99 a 50 mL steel jar and a 25 mm steel ball) for 3 min at 30 Hz (1800 rpm). 100 Biochar was stored in a drying oven at 105 ^{o} c until analysis. A single batch 101 of biochar was produced for each lignin type. Samples were weighed both 102 before and after pyrolysis to determine pyrolysis yield.

103 2.3. Sodium sulfate removal

104 As a secondary experiment, the impact of lignin Na2S04 content was 105 directly studied by removing Na2S04 from alkali-poplar95 lignin. To this 106 end, the alkali-poplar95 lignin was triple washed at a mass ratio of 1 part 107 original mass to 50 parts deionized water to remove Na2S04 and centrifuged 108 to separate after each washing cycle following established procedures [26]. 109 Lignin was freeze-dried after washing and then stored at 105 ^{o} c until py110 rolysis. Biochars were then prepared with this lignin and compared against 111 unwashed alkali-poplar95 biochar. Both biochars and washing residues were 112 measured with X-ray diffraction (XRD) and energy dispersive x-ray (EDX) 113 spectroscopy, as described in Section 2.4 to verify the removal of Na2S04 .114 For this set of experiments, biochar samples were produced in triplicate.

115 2.4. Lignin and biochar characterization

116 Biochar pyrolysis conditions were simulated in a thermogravimetric an117 alyzer (TGA, TA Instruments Q80001R) to examine the weight loss as a 118 function of temperature. Approximately 5 mg of each lignin was placed in a 119 HT-platinum TGA pan and heated from 30 °c to 1000 °c at a rate of 10 °c

120 min- under a 30 mL min I flow of nitrogen gas. Lignin thermal transitions
121 at low temperatures were examined with differential scanning calorimetry
122 (DSC, TA Instruments Discovery 2500). For DSC, approximately 5 mg of 123 each lignin was placed in a TZero DSC pan and heated from 30 °c to 400

124 °c at a rate of 10 °c min⁻¹.

125 Atomic species present in biochar were examined with EDX spectroscopy
126 with an Oxford Ultim Max EDX detector on a Zeiss SUPRA 55VP field
127 emission scanning electron microscope (FESEM). Based on the EDX results
128 (Supplemental Figure S7), C, H, N, S, Na, Mg, Ca, and K were selected for
129 quantified analysis. The C, H, N, and S content of all lignins and biochars
130 were characterized with combustion analysis by Atlantic Microlab Inc. (Nor131 cross, Georgia, USA). Lignin and biochar Na, Mg, Ca, and K content were

132 characterized with inductively coupled plasma optical emission spectrometry 133 (ICP-OES). Biochar and lignin samples were digested in trace metal grade 134 HN03 (Fisher Scientific, product #A509P500, Pittsburgh, PA USA) on a 135 Mars6 iWave digester at 220 °c with a ramp time of 15 min, a hold time 136 of 15 min, and under 800 psi of pressure. Dilution factors for ICP-OES are 137 shown in Supplemental Table S2. Digested samples and cation standards 138 were run in a matrix of 2% HN03 on a SpectroBlue ICP-OES in axial view 139 mode (high sensitivity). Oxygen content was then

calculated as the remain140 ing mass not accounted for by combustion analysis or ICP-OES. Organic

141 oxygen content was calculated with the assumption that Na2S04 was the
142 sole oxygen-containing inorganic species due to the lack of evidence for other
143 molecular species present. Na2S04 content was calculated based on the lower
144 stoichiometric value of either sodium or sulfur content (e.g., if 2 mol sodium
145 and 5 mol sulfur were present, 1 mol Na2S04 would be used). Given the low
146 concentrations of Ca, Mg, and K in all lignins (<0.06% for Ca, Mg, and K
147 content summed) and biochar (<0.41% for Ca, Mg, and K content summed), 148 this estimation represents the majority of inorganic oxygen present.

149 The chemical structure of all lignins and biochars was examined with 150 Fourier-transform infrared spectroscopy (FTIR) and XRD, and biochar was
151 additionally characterized with Raman spectroscopy. FTIR measurements
152 were performed on a ThermoFisher Nicolet iS50 FTIR spectrometer with a
153 Smart iTX attuned total reflectance (ATR) accessory with a diamond crystal.
154 Spectra were collected from wavenumbers of 600-4000 cm , at a resolution
155 of 4 cm^{1}, with 64 scans per sample. XRD of all lignins and biochars was
156 performed on a Bruker D8 Advance powder X-ray diffractometer with Kal,2 157 radiation, from 20 values of $10\text{-}70^{0}$ with a step size of 0.02^{0}. Raman spec158 tra were measured on a Horiba LabRam HR Evolution spectrometer with a
159 long-working distance objective and a frequency-doubled Nd:YAG laser
160 (wavelength of 532 nm) at a power of 1 mW. Carbon D and G peaks were 161 deconvoluted to determine Idg ratios, and XRD spectra were fit to determine 162 graphitic crystallite sizes as previously described [31, 32].
163 Gel permeation chromatography (GPC) was employed to determine the

number and weight average molar masses of the laboratory-isolated lignins, with acetylated samples utilized for the analysis [29]. An Agilent HPLC 1260 equipped with a Waters Styragel HR 4 (7.8 X 300 mm, Milford, MA, USA) column was used, with HPLC grade THF as the mobile phase with a 0.5 mL/min flow rate with UV detection at 280 nm and column temperature at 35 °c. As a reference, monodisperse polystyrene standards (Readycal, Fluka Analytical) were used in the range of 484 to 65,000 Da.

Lignin particle size was measured on a Malvern Mastersizer 2000 laser particle size analyzer with water as the dispersant and the assumption of non-spherical particles, as the biochar was ball milled. Before measurement, all samples except TCI alkaline and dealkaline lignins were placed in deionized water and sonicated for 5 min to disperse lignin particles. TCI alkaline and dealkaline lignins were placed directly into the particle size analyzer to limit dissolution. Biochar and lignin morphology were examined on a Zeiss SUPRA 55VP field emission scanning electron microscope (SEM) with an electron high tension voltage of 20 kV and a working distance of approximately 8.2 mm.

Biochar electrical conductivity was measured on 100 mg of biochar with a compressive guard electrode setup, as described in previous work [33]. Direct current resistance measurements were taken on a Keithly 2540 Sourcemeter from the point of first contact between the electrode and the biochar, as determined by the sourcemeter reaching its lower current limit until no more pressure could be applied. Biochar packing fractions were calculated assuming a skeletal density of 2 g/cm^3 for all biochars.

188 Biochar surface area and pore size distribution were characterized with 189 nitrogen sorption on a Micromeritics 3-Flex sorption analyzer 77 K for A95 190 biochar with and without Na2S04. The Brunauer-Emmett-Teller (BET) 191 model was used to determine surface area, and the non-local density func192 tional theory carbon slit pore model was used to determine the pore size 193 distribution. Gas sorption isotherms and pore size distributions are shown
194 in Supplemental Figure SIO.

195 2.5. Data analysis

196 All statistical analyses were performed in Minitab (vers. 19.2020.1, 197 Minitab LLC, State College, PA, USA), with a critical alpha set a priori to 198 0.05. Trends in shifts in the biochar elemental content with lignin elemental 199 content were analyzed with linear regression, with lignin elemental content 200 as the predictor variable and biochar elemental content as the response vari201 able. Impacts of lignin properties (H:C and O:C at. ratios, Na and S content, 202 molecular weight, particle size, dominant monomer, and lignin thermal tran203 sitions) on biochar electrical conductivity or in-plane graphic crystallite size 204 were analyzed with a forward selection regression model. The alpha value 205 for inclusion in the model was set a priori to 0.25. The impacts of biochar 206 treatments on biochar electrical conductivity were examined with analysis 207 of variance (ANOVA), including particle size treatment (commercial, milled, 208 or ground), washing to remove Na2S04 (washed, as prepared, or hydrolysis), 209 feedstock (commercial, poplar, or corn stover), or treatment type (hydroly210 sis, alkali, or commercial). Additionally, the impact of washing to remove 211 Na2S04 on alkali-poplar95 biochar electrical conductivity was examined with
212 one-factor ANOVA.

213 3. Results and Discussion

214 3.1. Lignin characterization

215 The lignins examined show a range of weight percentages of atomic species 216 present (Figure 1). Carbon is the most abundant element in all lignins, rang217 ing from 46.7 wt.% in TCI alkaline lignin to 61.7 wt.% in alkali-poplar 150

218 lignin. Additionally, all lignins show oxygen (31.5-43.4 wt.%) and hydrogen 219 (3.3-6.3 wt.%) content. Lignin inorganic content varies by isolation method. 220 All commercial lignins (TCI alkaline, TCI dealkaline, Sigma alkali) and un221 washed alkali lignins (alkali-poplar95) show the presence of sulfur (2.93-5.22 222 wt.%) and sodium (0.7-1.8 wt.%). In contrast, all other lignins show limited 223 sulfur content (0-0.31 wt.%) and sodium content (0.02-0.19 wt.%). Magne224 sium, calcium, and potassium are present in limited quantities in all lignins 225 (<0.1 wt.%).

226 As a result of the different methods used to reduce lignin particle size, 227 lignins show a range of median particle sizes (8.36-375 pm) and particle 228 size distributions (Supplemental Figure Sl). The three commercial lignins 229 (TCI alkaline, TCI dealkaline, Sigma alkali) all show approximately 100 gm 230 median particle sizes. All ball-milled lignins (alkali-poplar 150, hydrolysis231 corn, and alkali-corn140) show smaller particle sizes than other processing 232 methods at 8-34 gm median particle size. Lignins that were ground with 233 a pestle and mortar (alkali-poplar 145, alkali-poplar 115, and alkali-poplar95)

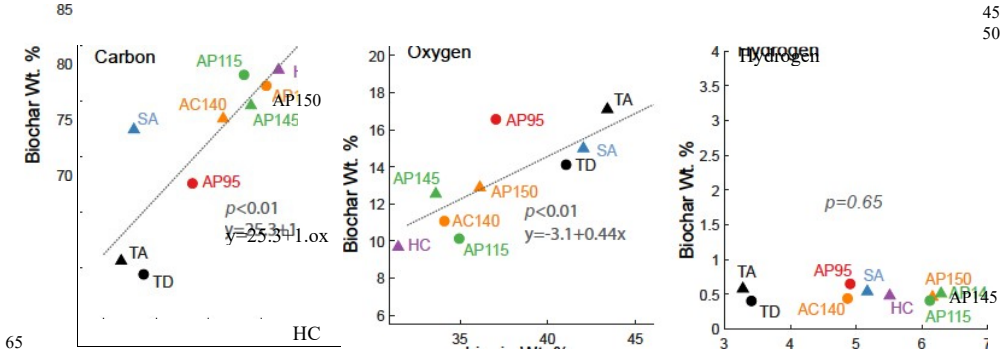

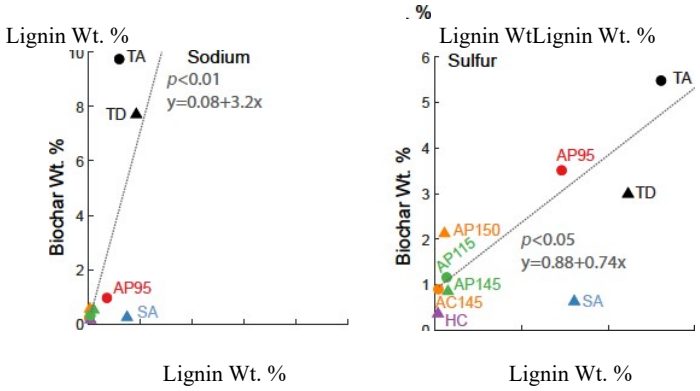

Figure 1: Comparison of weight % of C, H, O, Na, and S in all lignins before and after pyrolysis at 1100 ° c. Linear regression trend lines are shown for all elements with a significant relationship ($p < 0.05$).

were found to have the largest median particle sizes between 160 and 375 gm. Ball-milled and commercial lignins show narrower particle size distributions than ground samples. This range of median particle sizes allows for the testing of particle size as a variable previously identified as a key factor impacting biochar electrical conductivity [33].

FTIR spectra were used to broadly categorize the lignins by their dominant monomer (Supplemental Figure S2a and full peak assignments given in Supplemental Table S5). TCI alkaline, TCI dealkaline, alkali-poplar95, 115, 145, and 150 and hydrolysis-corn lignins show a stronger response for peaks associated with syringyl monomers at 1113 cm (aromatic C-H in-plane deformation) and 1323 cm $^{-1}$ (C-O in syringyl ring), while Sigma-Aldrich alkali 245 and alkali-corn140 lignins show a stronger response in peaks associated with guaiacyl monomers at 1032 cm (aromatic C-H in plane deformation) and 1263 cm $^{-1}$ (C-O in guaiacyl) [34]. Different lignin isolation procedures have limited impacts on monomer ratios. However, hydrolysis-corn shows a syringyl dominant spectra, while alkali-corn140 shows guaiacyl dominant spectra. Sigma-Aldrich alkali

and alkali-corn140, which show stronger guaiacyl 251 peaks, are isolated from spruce and corn, respectively, rather than the hard252 wood feedstocks used for the other lignins besides hydrolysis-corn [35, 36]. 253 While the primary Na2S04 peak (1112 cm ^{1}) overlaps with the primary sy254 ringyl peak, the presence of Na2S04 can be identified by the secondary S04 255 peak at 627 cm ^{I} [37], present as a strong peak in TCI alkaline, TCI dealka256 line, alkali-poplar95, and alkali-poplar 145 lignins, with weak peaks present 257 in Sigma-Aldirch alkali, alkali-poplar 115, and alkali-corn140 lignins. This 258 finding is supported by the relative concentrations of Na in these lignins, 259 with higher concentrations of Na present in TCI alkaline, TCI dealkaline, 260 and alkali-poplar95 lignins than others. The presence of Na2S04 in TCI 261 dealkaline, alkali-poplar95, alkali-poplar 115, and alkali-poplar 145 is further 262 supported by XRD patterns (Supplemental Figure S2b). Despite high levels 263 of Na and S and FTIR peaks attributed to S04, TCI alkaline does not show a 264 crystalline Na2S04 response in XRD, indicating the presence of amorphous 265 Na2S04. The range of organic elemental composition, amount of Na2S04 266 present, non-lignin contaminants, and dominant lignin monomers present in 267 these lignins allow for the impact of these properties on the resulting biochar 268 to be examined.

269 3.2. Lignin thermal transitions and biochar morphology

270 DSC curves of lignin show two distinct patterns of behavior when heated 271 (Supplemental Figure S3). The hydrolysis-corn lignin and washed alkali 272 lignins (alkali-poplar 145 and alkali-poplar 115) show strong, broad glass tran273 sitions at 110 ^{o} c. In contrast, the commercial lignins (TCI alkaline, TCI deal274 kaline, and Sigma-aldrich alkali), alkali-corn140 and alkali-poplar 150 show

275 sharp, weak glass transitions at approximately 150 ^{0}C. Above this second
276glass transition, lignins that are high in Na2S04 (as identified by elemental
277 composition, FTIR, and XRD) show a sharp transition that is attributed to
278 a polymorphic transition in Na2S04 [38]. Finally, at high temperatures, a 279 lignin softening transition is observed for all lignins [39, 40]. This transition 280 begins at a lower temperature (118-200 ^{0}C) for hydrolysis lignins than for 281 alkali or Kraft lignins (236-336 ^{0}C). In some lignins (alkali-poplar 115, 145, 282 and 150), the onset of thermal degradation can be observed as noise in the 283 DSC data above 300 ^{o}c.

284 The structure of the biochar post-pyrolysis varies as a result of these 285 differences in thermal transitions (Figure 2). In biochar produced from the 286 three commercial lignins (TCI alkaline, TCI dealkaline, and Sigma-Aldrich 287 alkali), a powdered structure is observed, with particle sizes similar to the 288 original lignins (Figure 2 and Supplemental Figure Sl). In alkali-corn140 289 and hydrolysis-corn biochars, a clumped particle structure is observed (Fig290 ure 2). In contrast, in alkali-poplar95, alkali-poplar 150, alkali-poplar 115, 291 and alkali-poplar 145 biochars, a "carbon foam" structure is observed. Op292 tical microscopy (Supplemental Figure S4) and SEM reveal that this "car293 bon foam" structure shows minimal distinction between individual particles 294 (Figure 2), with small (<200 nm) clumped, primarily carbon "cobbling" ob295 served via EDX and larger (1-2 um), higher sodium content particles observed 296 (Supplemental Figure S8). We hypothesize that this difference in behavior is 297 related to thermal transitions in the lignin. In lignins with a powdered struc298 ture (TCI alkaline and dealkaline, Sigma-Aldrich alkali) or weakly clumped

299 structure (hydrolysis-corn and alkali-corn140), DSC curves show weak or no 300 glass transition. In contrast, lignins with a continuous, "carbon foam" struc301 ture (alkali-poplar 150, 115, 145, and 95) all show strong glass transitions. 302 epending on the strength of these transitions, the structure of

the result303 ing biochar shifts from a powder similar in size to the original lignins to a 304 continuous material.

305 The formation of "carbon foam" structures could be attributed in part 306 to the melting of Na2S04. However, this behavior has previously been ob307 served at pyrolysis temperatures as low as 300 ^{0} C, below the melting tem308 perature of Na2S04 [41]. Further, this behavior is not observed in the two 309 highest Na2S04 content biochars - TCI alkaline and dealkaline. Notably, 310 all corn-derived lignins show clumped particle structures, all alkali-poplar 311 lignins show "carbon foam" structures, and all commercial lignins have pow312 dered structures. This finding indicates stronger softening transitions in 313 poplar-derived lignins than corn-derived lignins prior to the formation of 314 carbonized structures during pyrolysis. However, as previously observed 315 [42], lignin melting behavior shows a significant relationship with molecu316 lar weight ($p=0.002$), with the highest molecular weight lignins (TA, TD, 317 and SA Mw 28-60 kDa) showing no transition, moderate molecular weight 318 lignins (HC and AC140, Mw 10-11.4 kDa) showing packed powder mor319 phologies, and low molecular weight lignins, (AP 95, 115, 145, 150 and AP95320 Na, Mw 8-12.1 kDa) all showing continuous morphologies.

321 Notably, past studies have found that particle size may play an impor322 tant role in the graphitization of lignin during pyrolysis [7, 10]. Based on 323 the softening transitions observed and the resulting biochar morphology, we 324 hypothesize that in lignins with a strong softening transition, particle size 325 plays a limited role in resulting graphitization, as this size will have been 326 lost before most pyrolysis reactions. Particle size does not appear to play a 327 role in this transition, as similar lignins with large differences in size (such as 328 alkali-poplar 115 at 19 gm and alkali-poplar 145 at 375 pm) have these same

329 thermal transitions and form similar structures. However, particle size may 330 still play a role in the pyrolysis of lignins with a weak softening transition 331 (such as Sigma-Aldrich alkali and TCI alkaline and dealkaline lignins).

332 3.3. Biochar characterization

333Biochar yield varied between 21 and 45 wt.%, depending on lignin feed334 stock (Figure 3a). Typically, lignins with higher sodium content (TCI alka-

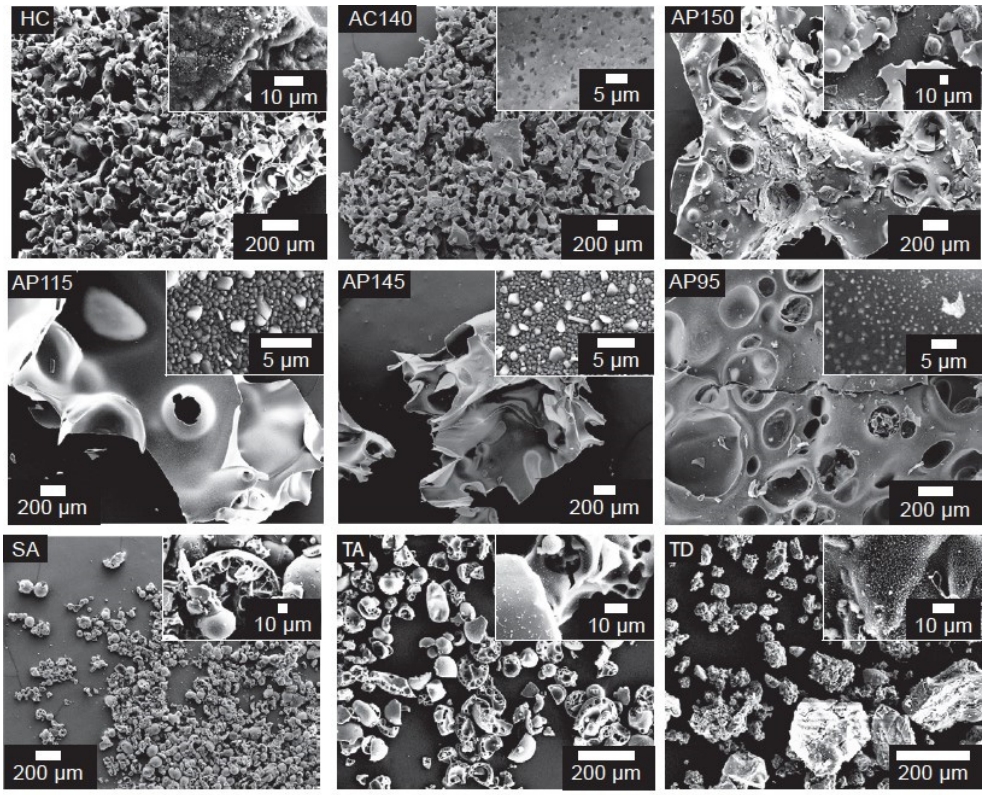

Figure 2: SEM micrographs of biochars produced from all lignins. Main images are at 50-250× magnification to highlight particle geometry, while insets are at 1000-3000× magnification to highlight surface features.

335 line, TCI dealkaline, Sigma-Aldrich alkali, and Alkali-poplar95) resulted in 336 higher biochar yields, which is attributed to the lack of reaction of Na2S04 337 during pyrolysis. In biochar that formed a carbon foam structure, the biochar 338 had expanded out of the alumina boat used. Therefore, some biochar was

339 lost during pyrolysis. The reactions that were responsible for these pyroly340 sis yields were examined with TGA, and final masses at 1000 °c generally

341 agreed with trends in biochar production yields (Figure 3b). At low temper-

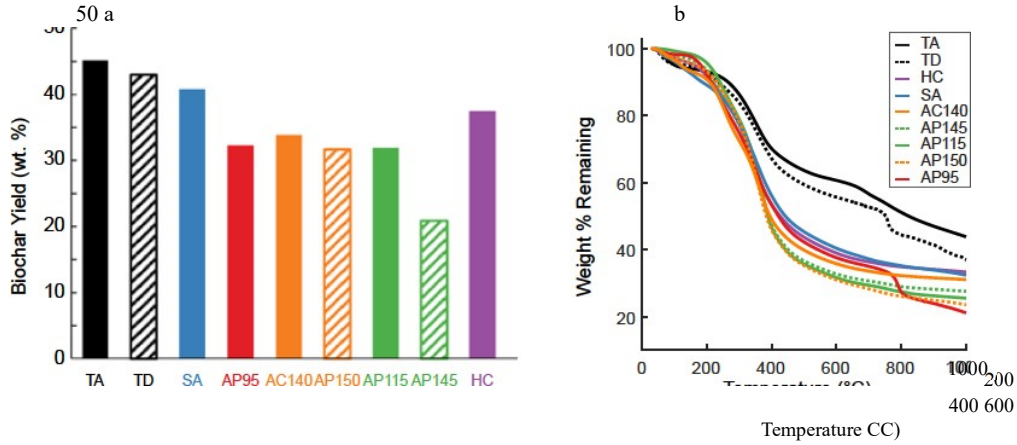

Figure 3: (a) Pyrolysis yield for each lignin. (b) TGA curves for each lignin under heating rates replicating tube furnace pyrolysis. Legend order shows the weight percent remaining at 1000 °c from highest to lowest.

342 atures (30-110 ^{0} C), all lignins show small mass losses (0.9-5.3%) associated 343 with moisture evaporation. At high temperatures, two distinct pyrolysis be344 haviors are observed - with the TCI alkaline and dealkaline lignins and the 345 alkali-poplar95 lignins all showing degradation in the 600-800 °c region. 346 In contrast, other lignins show only minor mass loss in this region. This 347 mass loss has previously been associated with the degradation of ether link348 ages into CO and C02 [43]. Additionally, these three lignins are some of 349 the highest in sodium and sulfur content (Figure 1), and decomposition of

350 Na2S04 has previously been observed at around 850 °c in the presence of

351 carbon [44]. Additionally, the presence of alkali metals, such as sodium, has 352 previously been observed to catalyze the decomposition of biomass during 353 pyrolysis, which could be responsible for the presence of this mass loss in

354 high Na2S04 lignins [25].

355 The carbon, oxygen, sodium, and sulfur content in the biochar is found 356 to be significantly impacted by the concentration of that element present 357 in lignin ($p < 0.05$, Figure 1). Carbon content shows a consistent increase 358 of approximately 25 wt.% with pyrolysis, attributed to loss of

oxygen and 359 hydrogen with pyrolysis. As a result of this shift, biochar carbon content is 360 additive to starting lignin carbon content (e.g., lignin that started at 50% 361 C results in approximately 75% C biochar). Only SA shows a meanin gful 362 variation from this trend, gaining approximately 35 wt.% carbon. Due to 363 limited evidence for the presence of carbon-containing inorganic compounds, 364 this carbon is assumed to be entirely organic. We note that some inorganic 365 species, such as Ca, were found via ICP-OES, which would commonly be 366 present in biomass as carbon-containing species (e.g., CaC03), which could 367 indicate the presence of some inorganic carbon [16], but also could be present 368 as CaO or CaS04 following thermal decomposition of CaC03.

369 Similarly, biochar oxygen content increases with increasing lignin oxygen 370 content, however, at a slower rate than carbon, with approximately 44% 371 of the lignin oxygen remaining after pyrolysis on average. Biochar organic 372 oxygen content is expected to play an important role in biochar electrical 373 conductivity [10, 20]. Lignin hydrogen content was not found to have a 374 significant impact on biochar hydrogen content ($p = 0.65$). All biochars 375 showed hydrogen content of approximately 0.5 wt.%, while lignin hydrogen 376 content varied from 3.3-6.3 wt.%. This similar hydrogen content indicates 377 that in these biochars, H:C atomic ratios, and therefore inferred graphitic 378 structure diameters [45], are driven primarily by carbon content. Biochar 379 and lignin atomic compositions are tabulated in Supplemental Tables S3 and

381 All biochars showed low (<0.2 wt.%) Mg, Ca, and K concentrations (Sup382 plemental Table S4). In contrast, biochars from acidification processes with383 out washing steps (TCI alkaline and dealkaline, alkali-poplar95, and Sigma384 Aldrich alkali) show high concentrations of Na and S. These concentrations 385 are found to be typically significantly higher than the

concentration of sodium 386 or sulfur in the lignin feedstock ($p < 0.01$ and < 0.05 for Na and S, respec387 tively). In the case of sodium, this increase in concentration (3.2><) roughly 388 matches the change in mass (average yield of 35%, Figure 3), indicating that 389 minimal sodium has reacted off during pyrolysis. Molar ratios of sodium 390 to sulfur in biochar show differing shifts depending on the lignin feedstock, 391 which indicates the presence of multiple sodium and sulfur-containing com392 pounds or organic sulfur. However, XRD and FTIR spectra of both lignin 393 and biochar show Na2S04 as the predominant form of both sodium and sul394 fur in all biochar. A meaningful portion of biochar and lignin oxygen is 395 inorganic, with between 3 and 35% of total oxygen present in Na2S04 based 396 on sodium content (Supplemental Table S4).

397 Sigmoidal electrical percolation behavior is observed in all biochars as 398 they are compressed (Figure 4b). At low compressions, all biochars show 399 highly resistive behavior, as the non-conductive air dominates the unpacked

400 powder. At a packing fraction of approximately 0.25, the percolation thresh401 old is reached, and electrical conductivity rapidly increases. The percolation 402 threshold is similar for all biochars, indicating similar particle geometry and 403 packing despite differences in the structure after pyrolysis but before ball 404 milling. The peak electrical conductivity of all biochars varied by two orders 405 of magnitude between biochars, from 0.19 S/cm for TCI alkaline biochar 406 to 18.9 S/cm for alkali-poplar95 biochar. These variations are consistent 407 with what has previously been observed for pyrolysis of lignin at 1100 ^{o} c

408 with electrical conductivity measured with the same method and in the mid409 dle of a range of values previously observed for all lignin-derived biochars 410 [10]. The upper range (>10 S/cm) of these conductivities are comparable 411 to those of electrically conductive carbon blacks [33, 46], and are suffcient 412 for many electrical applications, including anti-static

materials, sensors, and 413 conductive additives in batteries. At a pyrolysis temperature of 1100 ^{0} C, no 414 further increase in electrical conductivity is expected with further increases 415 in pyrolysis temperature [21].

416 A number of factors impact biochar electrical conductivity: the size of 417 graphitic crystallites, displacements and deformations on those crystallites, 418 biochar surface groups, and biochar particle size [10, 20, 21]. XRD patterns 419 of the biochar show variation in the in-plane size of graphitic crystallites (La) 420 but minimal shifts in size or distance between sheets in the stacking direction 421 (Lc and d002) with an average and standard deviation of 1.2 ± 0.1 graphene 422 planes per crystallite across all samples. The in-plane size of graphitic crystal423 lites varies from 3.4 Å for TCI dealkaline biochar to 41 Å for alkali-poplar 115-

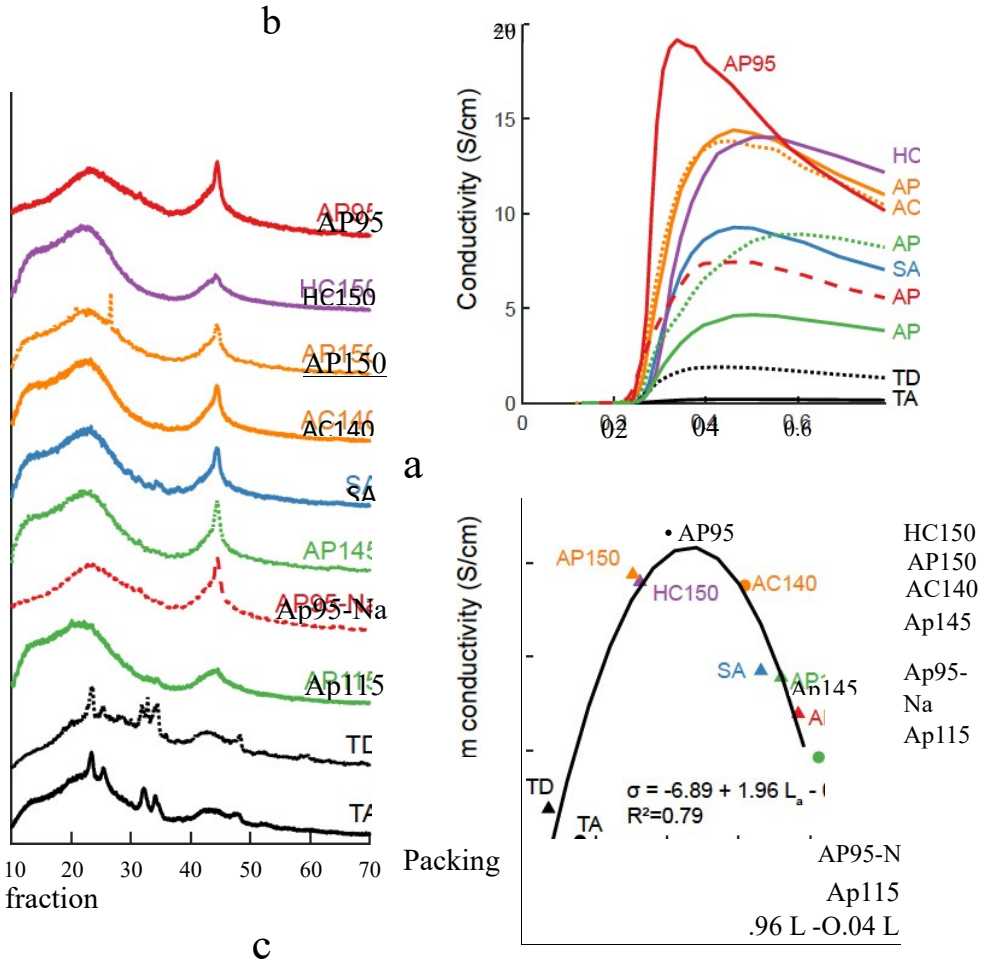

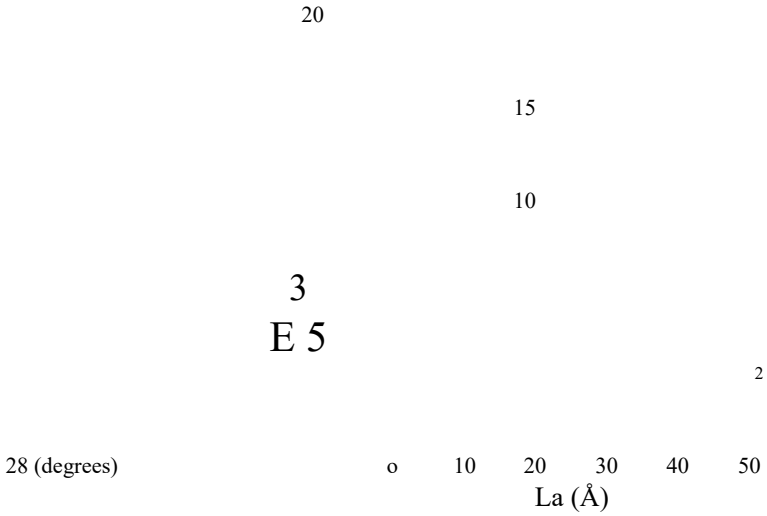

Figure 4: Characterization of biochar graphitic structure and electrical conductivity showing (a) XRD patterns. Lines are stacked in order of maximum electrical conductivity from highest (top) to lowest (bottom), (b) electrical conductivity as a function of packing fraction, and (c) relationship between in-plane graphitic crystallite size and electrical conductivity. Error bars in (b) and (c) represent the maximum and minimum values of peak conductivity for three samples from a comparison of AP95 with and without Na2S04, and the point or line represents the median value.

424 biochar. TCI alkaline and dealkaline biochar show poor fits of XRD patterns 425 relative to other biochar, which is attributed to the high contribution of in426 organic components to the XRD pattern in these biochars, which were not

427 included in the fitting procedure (Supplemental Figure S6a and b). Minimal
428 shifts are observed in Raman spectra between samples (Supplemental Fig429 ure S5). All biochars show the typical D and G peaks that are typical for

430 non-graphitizing carbons [31]. The intensity ratio of these peaks (Idg) ranges

431 from 1.03-1.18. In TA, an additional peak is observed at 1058 cm^{1}, which
432 is attributed to Na2S04 (Supplemental Figure S5) [47]. TCI alkaline and

433 dealkaline biochars have a shallower valley between the D and G peaks than

434 other biochars. The ratio of this valley depth to the height of the G-peak has

previously been correlated with the degree of graphitization [48]. Combined with limited 101 peaks in the XRD patterns of TCI alkaline and dealkaline biochars and low electrical conductivity, this finding demonstrates that these 438 biochars have lower graphitization than the other biochars examined. A full 439 summary of fit values from XRD and Raman is given in Table 2.

Despite the range of properties and electrical conductivity identified 441 herein, no statistically significant relationship was found with a linear re442 gression between any of the examined lignin properties (H:C and O:C at. ratios, Na and S wt. %, molecular weight, particle size, dominant monomer, and lignin thermal transitions) and biochar electrical conductivity ($p > 0.05$ for all, Figure 5). Similarly, one-factor ANOVAs found no statistically sig446 nificant differences ($p > 0.05$ for all) between treatment groups, including 447 particle size treatment (commercial, milled, or ground), washing to remove 448 Na2S04 (washed, as prepared or received, or hydrolysis), feedstock (commer-

Table 2: Calculated XRD (in-plane graphitic crystallite size (La), out-of-plane graphitic crystallite size (Lc), crystallite aspect ratio (La/Lc), and space between planes (d) and Raman values (Intensity ratio of fit d peak go g peak IDG and width of G peak (WG)) and peak electrical conductivity for all biochar. Complete Raman spectra are given in Supplemental Figure S5, and XRD fits are given in Supplemental Figure S6.

	La(Å)	Lc (Å)	La/Lc		IDG	WG	Conductivity (S/cm)
TCI alkaline	7.8	4.6	1.7	4.0	1.1	148.0	0.2
TCI dealkaline	3.4	5.2	0.7	3.7	1.1	133.9	1.9
Sigma-Aldrich alkali	33.1	5.0	6.6	4.1	1.1	151.2	9.3
Hydrolysis-corn	16.2	4.9	3.3	4.1	1.2	147.7	14.0
Alkali-corn140	15.2	4.3	3.5	4.4	1.1	153.9	14.4
Alkali-poplar 150	30.9	4.6	6.7	4.3	1.1	137.5	13.8
Alkali-poplar 115	41.2	4.9	8.4	4.2	1.0	146.8	4.6
Alkali-poplar145	35.9	4.9	7.3	4.3	1.1	146.0	8.9
Alkali-poplar95	19.5	5.1	3.8	4.4	1.2	146.1	18.5
Alkali-poplar95-Na	38.3	4.0	9.5	3.8			7.0

449 cial, poplar, or corn stover), or treatment type (hydrolysis, alkali, or com450 mercial). This lack of significance holds even when processing methods and feedstock for commercial lignins are ungrouped, and feedstock is assumed to

452 be mixed wood for TCI alkaline and dealkaline lignin, softwood for Sigma453 Aldrich alkali lignin, and treatment type is assumed to be alkaline for TCI 454 alkaline and dealkaline lignin and alkali for Sigma-Aldrich alkali lignin.

455 However, when examining the relationship between lignin properties

456 and biochar in-plane graphitic crystallite size (La, Supplemental Figure 457 S8)), a significant relationship was observed with lignin H:C atomic ratio 458 ($p = 0.042$). This relationship shows an increasing graphitic crystallite size

459 with an increasing H:C ratio. Notably, despite a wide range of hydrogen con460 tent in the lignin feedstocks, the biochar produced shows limited variation in 461 hydrogen content (Figure 1). This finding indicates that feedstock hydrogen

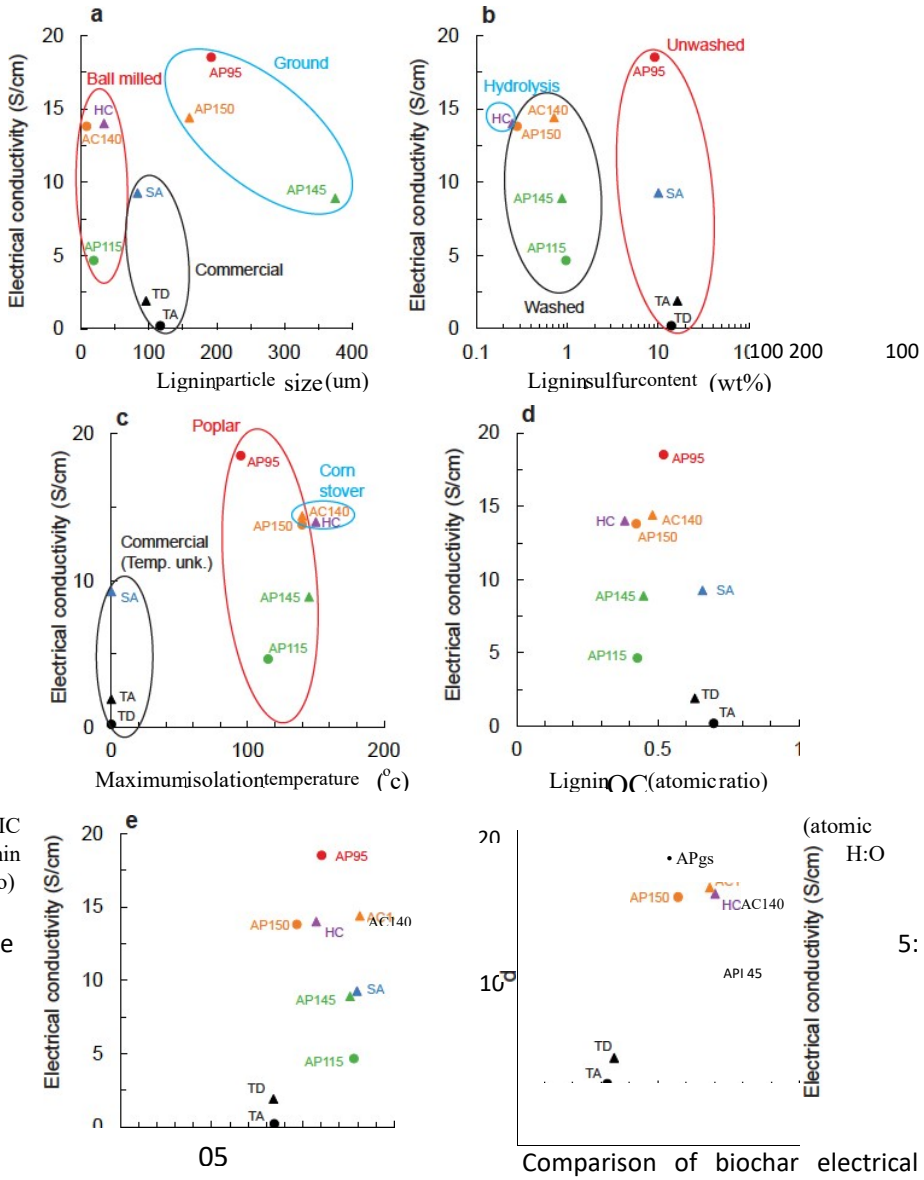

Figure 5: Comparison of biochar electrical conductivity with (a) lignin particle size, (b) lignin sulfur content, (c) lignin max. isolation temperature, (d) lignin organic O:C ratio, (e) lignin H:C ratio, and (d) lignin organic H:O ratio. Labeled groups are treatment groups.

462 content has a limited effect on the final molecular structure. Instead, hydro463 gen plays a role in the pyrolysis reactions that lead to the formation of those 464 structures. This finding is consistent with past models of biomass pyroly465 sis, which state that when insuffcient hydrogen is present in a feedstock to

466 react with oxygen, which forms distortions in the graphitic structure, these 467 distortions persist, even at high pyrolysis temperatures, limiting the

possi468 ble degree of graphitization of the feedstock [20]. As oxygen content shows 469 lower variation between lignin feedstocks (O:C ratios of 0.38-0.70, relative 470 to H:C ratios of 0.84-1.31), the hydrogen content is the primary driver of 471 variation in graphitization of the lignin feedstocks examined. Future work 472 examining a wider range of lignin oxygen content could better highlight the 473 role of oxygen in these reactions. As a result, it may be preferable to produce 474 lignin with higher guaiacyl monomer content (H:O at. ratio of 4) rather than 475 syringyl dominant lignin (H:O at. ratio of 3.3). We note, however, that no 476 relationship is observed between the biochar H:O ratio or in-plane graphitic 477 crystallite size and the dominant monomer in this work, and relatively few 478 guaiacyl-dominant lignins (AC140 and SA) were examined. Further, those 479 two lignins show relatively small differences in electrical conductivity, both 480 within the upper half of electrical conductivities examined (14.4 and 9.3 S/cm 481 for AC140 and SA, respectively).

482 Alkali-poplar95 biochar, as the highest electrical conductivity biochar, 483 was selected for further testing to examine the impact of inherent Na2S04 484 on lignin-derived biochar electrical conductivity and carbon structure. After 485 washing to remove Na2S04 from alkali-poplar95 (alkali-poplar95-Na) , limited 486 sulfur or sodium content was observed via EDX, and no Na2S04 peaks were 487 observed via XRD (Supplemental Figure S9). An ANOVA assessing the 488 impact of Na2S04 removal treatment on alkali-poplar95 biochar electrical 489 resistivity found a statistically significant impact from Na2S04 treatment 490 ($p < 0.01$). Alkali-poplar95 biochar had an average electrical conductivity 491 of 17 ± 1.6 S/cm (Figure 4 and Supplemental Figure S9). With Na2S04 492 removed, electrical conductivity was reduced to 7.0 ± 0.5 S/cm.

493 The mechanisms behind this difference in electrical conductivity were fur494 ther explored with XRD, finding a meaningful increase in crystallite size

of 495 the graphitic 10 plane (La) with the removal of Na2S04 (Figure 4a and Table

496 2). Alkali-poplar95 biochar shows an in-plane crystallite size of 16.2 Å on

497 average. With the removal of Na2S04, in-plane crystallite size meaningfully 498 increases to 38.3 Å. In contrast, crystallite size in the stacking 002 direc499 tion (Lc) only shows minor shifts between 4-5 Å for both treatments with a 500 distance of approximately 4 Å between each layer. Importantly, this finding 501 indicates that the presence of Na2S04 inhibits graphitization in lignin-derived 502 biochars. Further, the BET surface area of the biochar decreases from 27.10 503 m^2 /g in alkali-poplar95 with Na2S04 to 8.16 m^2 /g when Na2S04 is removed. 504 This decrease in surface area with Na2S04 removal is driven by a decrease 505 in pores with a width of less than 35 Å (Supplemental Figure SIOb). The 506 combination of increased graphitic crystallite size and decreased BET surface 507 area of smaller pores is consistent with past findings of micro-pore closure 508 with increasing graphitization [49]. This is further supported by increased 509 hysteresis during desorption in akali-poplar95 relative to with Na2S04 re510 moved, indicating the presence of constricted pores when Na2S04 is present, 511 that are closed when Na2S04 is not present [49].

512 Beyond alkali-poplar95 with and without Na2S04 removal, individual

513 comparisons can be made based on similar lignins with individual differences

514 in processing. Alkali-poplar 150 and alkali-corn140 were processed similarly,

515 but different feedstocks (poplar and corn Stover) and particle sizes (34 gm 516 and 160 pm), but the resulting biochars have similar electrical conductivi517 ties (13.8 and 14.4 S/cm). However, they have different graphitic crystallite

518 sizes with an in-plane graphitic crystallite size of 15.2 and 30.9 Å for corn

519 and poplar, respectively. Alkali-poplar95, which was processed similarly to
520 alkali-poplar 150 but with a lower treatment temperature and no washing to
521 remove Na2S04, resulted in higher electrical conductivity. Similarly, alkali522 poplar 115 and alkali-poplar 145 have similar processing, chemical content, 523 and graphitic crystallite size with differences in treatment temperature, but 524 alkali-poplar 145 shows higher electrical conductivity than alkali-poplar 115.

525 The two corn-stover-derived lignins examined (hydrolysis-corn and alkali526 corn140) show broadly similar properties despite the different processing
527 methods used; as alkali-corn140 was washed to remove Na2S04, both have
528 low sodium and sulfur content, and both lignins were ball milled and there529 fore show similar particle sizes. When alkali-poplar95 is washed to remove 530 Na2S04, the electrical conductivity decreases, and the in-plane graphitic 531 crystallite size increases to be comparable to alkali-poplar 115 and alkali532 poplar 145. These two lignins were processed similarly to alkali-poplar95, ex533 cept they were washed to remove Na2S04, indicating that this washing step 534 drives the large differences between these three otherwise similar lignins.

535 As biochar graphitic crystallite size only meaningfully varies in the in536 plane direction, the aspect ratio of graphitic crystallites varies greatly be537 tween different biochars. This shift in graphitic crystallite size is found to 538 play a key role in biochar electrical conductivity. A strong quadratic re539 lationship is found between in-plane graphitic crystallite size and biochar 540 conductivity ($p < 0.01$, Figure 4c). This relationship peaks in electrical con541 ductivity at an in-plane graphitic crystallite size of 23 Å. We propose two 542 mechanisms for this behavior, which expand on the previously developed 543 quasi-percolation model for biochar electrical conductivity [21, 30]. At small 544 in-plane graphitic crystallite sizes, such as are found in TCI alkaline and

545 dealkaline biochar, limited graphitization has occurred due to the presence 546 of high quantities of Na,2S04 as indicated by elemental composition, XRD, 547 and Raman spectroscopy. Graphitic crystallites in these materials have lim548 ited electrically conductive contact between crystallites and are separated by 549 lower electrical conductivity displaced graphitic carbon, as predicted by pre550 vious quasi-percolation models [21]. As the size of these crystallites expands, 551 such as in alkali-corn-140 and hydrolysis-corn biochar, there are increased 552 contacts between electrically conductive regions. These contacts reach a 553 maximum at in-plane graphitic crystallite sizes of approximately 23 Å, cor554 responding to a graphitic crystallite aspect ratio of 3.8 La/Lc. Above this 555 contact, the high aspect ratio and the random orientation of graphitic crys556 tallites [50] limit contacts between the crystallites, resulting in lower electrical 557 conductivity. This proposed behavior matches those previously observed for

558 percolation in packed powder systems, where higher aspect ratios result in 559 reduced electrical conductivity [46]. In addition, the graphitic crystallite size 560 that results in the highest biochar electrical conductivity is similar to that 561 of highly electrically conductive carbon blacks [11]. This similarity suggests 562 that similar mechanisms for crystallite packing occur in petroleum-derived 563 carbon black.

564 A complex series of multi-phase reactions is observed during pyrolysis, 565 driven by the melting behavior of some lignins at low temperatures, melting 566 of Na2S04 at high temperatures, and secondary reactions of liquid oil and tar

567 pyrolysis products back to solid biochar. No statistically significant trends 568 were observed in electrical conductivity or graphitic crystallite size based on 569 the melting behavior of the biochar. However, this may in part be due to the

570 compounding of other effects, as two of the lignins with no observed melting 571 behavior (TA and TD) were also the highest in Na2S04, and the two lignins 572 that showed clumped-powder behavior (HC and AC140) were the lowest in 573 Na2S04 content, while continuous morphologies showed a range of Na2S04 574 content. Further, at 1000 ^{0}C, lignins that showed no melting behavior showed 575 the highest yields at 200-1000 ^{o}c via both TGA and pyrolysis yields at 1100 576 ^{o}c (Figure 3), followed by clumped powder morphologies, with continuous
577 morphologies having the lowest yields. While previous studies have observed 578 increased decomposition at low pyrolysis temperatures in lignins that show 579 melt behavior [42] , an alternative explanation is that non-melting lignins have 580 a higher molecular weight, which is also correlated with increased biochar 581 yields, rather than the melting itself. Further, at present, it is unknown how 582 these shifts in low-temperature behavior impact the formation of graphitic 583 structures at pyrolysis temperatures above 900 ^{0}C. Critical examination of 584 this phenomenon, controlling for the identified compounding factors herein, 585 could provide additional insight into which lignin isolation procedures and 586 lignin properties provide the best feedstock for differing carbon applications.

587Multiple structures of Na2S04 were observed via SEM-EDX, with Na2S04 588 being present as both a "skin" on the outside of the biochar and integrated as 589 approximately 1 pm structure between the majority carbon structures (Sup590 plemental Figure S8). The impacts of Na2S04 melting on lignin pyrolysis, 591 as well as the mechanisms responsible for the herein observed shifts in car592 bon structure with Na2S04 presence, is a particularly interesting area for 593 further study. A better understanding of these mechanisms would allow for 594 the carbon structures of lignin-derived carbons to be better optimized for 595 specific applications. Past work on molten salt interactions during pyrolysis 596 has shown molten salt to impact carbon structures [51, 52], and a better 597 understanding of these interactions in lignin pyrolysis is

needed to modify 598 the structures of lignin-derived carbons to specific applications.

599 This study highlights the development of low aspect ratio graphitic crys600 tallites but well-graphitized carbon structures as a potential method to in601 crease the electrical conductivity of carbons produced from non-graphitizing 602 feedstocks. Future work should examine if biochar could be produced with 603 limited disordered and displaced graphitic content but with graphitic crys604 tallite aspect ratios approaching 1, as higher electrical conductivities of the 605 bulk material may be possible. Importantly, this work demonstrates that 606 Na2S04 levels in lignin can be controlled to selectively control graphitization 607 of lignin-derived biochar and tune graphitic crystallite size and electrical 608 conductivity to a desired application. Modification of pore size distributions 609 and surface area via selective Na2S04 removal can tune these critical factors 610 for carbon applications such as battery active materials [53]. Further, in 611 future work, multiple variables, such as pyrolysis temperature and Na2S04 612 level, could be tuned to examine combinations that maximize highly elec613 trically conductive carbon production while minimizing energy consumption 614 during production. Given the strong performance previously demonstrated 615 by lignin-derived carbons across multiple applications [7, 11, 14, 15], this 616 work provides key guidance on feedstock selection and modification to meet 617 the requirements of carbons as commercial application of lignin-derived car618 bons continues to grow. However, the additional processing step required 619 to remove Na2S04 would be expected to introduce additional costs, and the 620 benefits of additional tuning of the carbon properties should be carefully 621 evaluated against these costs. Process considerations, such as tuning the 622 amount of NaOH added during delignification and the sulfuric acid addition

623 during precipitation of alkali lignins or selection of sulfur-free processes (e.g.,

hydrolysis), could allow for tuning the sodium sulfate content of lignin to a desired carbon application without additional washing steps. However, these process changes would need to be carefully evaluated against the outputs of the biorefinery process as a whole. The simple water washing method demonstrated herein would be expected to be lower cost compared to other methods to tune biomass-derived carbon properties such as iron catalysts, which must be removed with acid washes [15] or activation processes that consume more costly activation agents, such as KOH [14].

4. Conclusions

This work highlights that all lignins are not equal for producing electrically conductive biochar, with a 100-fold difference in electrical conductivity between the most and least conductive biochar measured. The wide range of electrical conductivities observed herein for lignin-derived biochars confirms that similar ranges observed between past studies are not exclusively due to differences in biochar production or electrical conductivity measurement methods. Na_2SO_4 content in lignin is identified as a significant factor in lignin-derived biochar carbon structure, with Na_2SO_4 inhibiting the formation of larger graphitic crystallites. However, the aspect ratio of graphitic crystallites in lignin-derived biochar plays an important role in the electrical conductivity of the resulting biochar, with a quadratic relationship observed with a maximum electrical conductivity at an aspect ratio of 4. Many of the examined lignin-derived biochars have higher aspect ratios, resulting in lower electrical conductivity despite larger graphitic crystallites. Therefore, the presence of moderate amounts of Na_2SO_4 can be used to selectively tune the carbon structure in lignin-derived carbons and maximize electrical conductivity. This finding builds on past quasi-percolation

models that describe 650 the packing of graphitic crystallites within carbon particles as an important 651 contributor to their bulk electrical conductivity and can help to inform the

652 development of future electrically conductive, non-graphitizing carbons.

653 Acknowledgements

654 We would like to thank Dr. Nicholas P. Stadie and Dalton Compton 655 for their assistance with gas sorption measurements. S.K.'s contribution was 656 funded in part through a Ph.D. Fellowship from the Environmental Research 657 and Education Foundation. This work was performed in part at the Montana 658 Nanotechnology Facility, a member of the National Nanotechnology Coor659 dinated Infrastructure (NNCI), which is supported by the National Science

660 Foundation (Grant #ECCS-1542210). D.B.H., B.S., V.E.B., and D.N.D.'s 661 contribution was based upon work supported by the U.S. Department of En662 ergy's Offce of Energy Effciency and Renewable Energy (EERE) under the 663 Bioenergy Technologies Offce Award # DE-EE0008148. This work repre664 sents the views of the authors, not necessarily those of the funders.

665 References

666 [1] Maria-Magdalena Titirici, Robin J. White, Nicolas Brun, Vitaliy L. 667 Budarin, Dang Sheng Su, Francisco del Monte, James H. Clark, and 668 Mark J. MacLachlan. Sustainable carbon materials. Chem. Soc. Rev., 669 44:250-290, 2015. doi: 10.1039/C4CS00232F.

670 [2] Sabornie Chatterjee and Tomonori Saito. Lignin-derived advanced car671 bon materials. ChemSusChem, 8:3941—3958, 12 2015. ISSN 1864-564X. 672 doi: 10.1002/CSSC.201500692.

673 [3] D. S. Bajwa, G. Pourhashem, A. H. Ullah, and S. G. Bajwa. A concise 674 review of current lignin production, applications, products and their 675 environmental impact. Industrial Crops and Products, 139: 111526, 11 6762019. ISSN 0926-6690. doi: 10.1016/J.1NDCROP.2019.111526.

677[4] Jason K. Hansen, Jacob J. Jacobson, Kara G. Cafferty, Patrick Lamers, 678and Mohammad S. Roni. Quantifying supply risk at a cellulosic biore679 finery. 33rd International Conference of the System Dynamics Society, 6807 2015. URL https://www.osti.gov/biblio/1357903.

681 [5] Julia Wenger, Verena Haas, and Tobias Stern. Why can we make any682 thing from lignin except money? towards a broader economic perspec683tive in lignin research. Current Forestry Reports, 6:294—308, 12 2020.

684 ISSN 21986436. doi: 10.1007/S40725-020-00126-3.

685[6] Richard J. A. Gosselink. Lignin as a Renewable Aromatic Resource for 686 the Chemical Industry. PhD thesis, Wageningen University, 2011. URL 687 https://www.proquest.com/dissertations-theses/lignin-as-renewable 688 aromatic-resource- chemical/ docview/ 2568538894/se- 2?accountid=

689 28148.

690 [7] William J. Sagues, Ankush Jain, Dylan Brown, Salonika Aggarwal, An691 tonio Suarez, Matthew Kollman, Seonghyun Park, and Dimitris S. Ar692 gyropoulos. Are lignin-derived carbon fibers graphitic enough? Green 693 Chemistry, 21:4253—4265, 8 2019. ISSN 14639270. doi: 10.1039/ 694 C9GC01806A.

695 [8] Muhannad Al Aiti, Dieter Jehnichen, Dieter Fischer, Harald Brünig, 696 and Gert Heinrich. On the morphology and structure formation of 697 carbon fibers from polymer precursor systems. Progress in Materi698 als Science, 98:477—551, 10 2018. ISSN 0079-6425. doi: 10.1016/ 699 J.PMATSC1.2018.07.004.

[9] Xiaoyu Wu, Junhua Jiang, Chongmin Wang, Jian Liu, Yunqiao Pu, Arthur Ragauskas, Songmei Li, and Bin Yang. Lignin-derived electrochemical energy materials and systems. Biofuels, Bioproducts and Biorefining, 14:650-672, 5 2020. ISSN 1932-1031. doi: 10.1002/BBB.2083.

[10] Seth Kane, Rachel Ulrich, Abigail Harrington, Nicholas P. Stadie, and Cecily Ryan. Physical and chemical mechanisms that influence the electrical conductivity of lignin-derived biochar. Carbon Trends, page 100088, 2021. ISSN 2667-0569. doi: 10.1016/j.cartre.2021.100088.

[11] Seth Kane, Aksiin Storer, Wei Xu, Cecily Ryan, and Nicholas P. Stadie. Biochar as a renewable substitute for carbon black in lithium-ion battery electrodes. ACS Sustainable Chemistry Engineering, 10(37):12226— 12233, 2022. doi: 10.1021/acssuschemeng.2c02974.

[12] Haiping Yang, Rong Yan, Hanping Chen, Dong Ho Lee, and Chuguang Zheng. Characteristics of hemicellulose, cellulose and lignin pyrolysis. Fuel, 86:1781-1788, 8 2007. ISSN 0016-2361. doi: 10.1016/ J.FUEL.2006.12.013.

[13] Michael R Snowdon, Amar K Mohanty, and Manjusri Misra. A study of carbonized lignin as an alternative to carbon black. ACS Sustainable Chemistry & Engineering, 2: 1257—1263, 2014. doi: 10.1021/sc500086v.

[14] Kai Chen, Zi-Jing He, Zhi-Hua Liu, Arthur J. Ragauskas, Bing-Zhi Li, and Ying-Jin Yuan. Emerging Modification Technologies of Lignin-based Activated Carbon toward Advanced Applications. ChemSusChem, 15 201284, 2022. ISSN 1864-564X. doi: 10.1002/cssc.202201284.

[15] William J. Sagues, Junghoon Yang, Nicholas Monroe, Sang-Don Han, Todd Vinzant, Matthew Yung, Hasan Jameel, Mark Nimlos, and Sunkyu Park. A simple method for producing bio-based anode materials for

lithium-ion batteries. Green Chemistry, 22: 7093—7108, 10 2020. ISSN 1463-9270. doi: 10.1039/DOGC02286A.

[16] Nancy Chen and Srikanth Pilla. A comprehensive review on transforming lignocellulosic materials into biocarbon and its utilization for composites applications. Composites Part C: Open Access, 7: 100225, 3 2022. ISSN 2666-6820. doi: 10.1016/J.JCOMC.2021.100225.

[17] Wenli Zhang, Xueqing Qiu, Caiwei Wang, Lei Zhong, Fangbao Fu, Jiahao Zhu, Zejie Zhang, Yanlin Qin, Dongjie Yang, and Chunbao Charles Xu. Lignin derived carbon materials: current status and future trends. Carbon Research, 1(1):14, July 2022. ISSN 2731-6696. doi: 10.1007/s44246-022-00009-1.

[18] Amar K. Mohanty, Singaravelu Vivekanandhan, Oisik Das, Lina M. Romero Millån, Naomi B. Klinghoffer, Ange Nzihou, and Manjusri Misra. Biocarbon materials. Nature Reviews Methods Primers, 4(1): 1-21, March 2024. ISSN 2662-8449. doi: 10.1038/s43586-024--00297-4.

[19] Janea Köhnke, Harald Rennhofer, Helga Lichtenegger, Arunjunai Raj Mahendran, Christoph Unterweger, Batirtze Prats-Mateu, Notburga Gierlinger, Elisabeth Schwaiger, Arnulf Kai Mahler, Antje Potthast, and Wolfgang Gindl-Altmutter. Electrically conducting carbon microparticles by direct carbonization of spent wood pulping liquor. ACS Sustainable Chemistry & Engineering, 6:3385—3391, 3 2018. ISSN 21680485. doi: 10.1021/ACSSUSCHEMENG.7B03582.

[20] John S. McDonald-Wharry, Merilyn Manley-Harris, and Kim L. Pickering. Reviewing, combining, and updating the models for the nanostructure of non-graphitizing carbons produced from oxygen-containing precursors. Energy and Fuels, 30:7811—7826, 10 2016. ISSN 15205029. doi: 10.1021/acs.energyfuels.6b00917.

753 [21] Ying Shao, Chamseddine Guizani, Philippe Grosseau, Didier Chaussy, 754 and Davide Beneventi. Biocarbons from microfibrillated cellu755 lose/lignosulfonate precursors: A study of electrical conductivity de756 velopment during slow pyrolysis. Carbon, 129:357—366, 4 2018. ISSN 757 00086223. doi: 10.1016/j.carbon.2017.12.037.

758 [22] Singaravelu Vivekanandhan, Manjusri Misra, and Amar Kumar Mo759 hanty. Microscopic, structural, and electrical characterization of the 760 carbonaceous materials synthesized from various lignin feedstocks. Jour761 nal of Applied Polymer Science, 132:41786, 4 2015. ISSN 1097-4628. doi:
762 10.1002/APP.41786.

763 [23] J. Rodriguez-Mirasol, T. Cordero, and J. J. Rodriguez. High764 temperature carbons from kraft lignin. Carbon, 34:43—52, 1 1996. ISSN 765 00086223. doi:10.1016/0008-6223(95)00133-6.

766 [24] Gang Xiao, Mingjiang Ni, Rui Xiao, Xiang Gao, and Kefa Cen. Cat767 alytic carbonization of lignin for production of electrically conductive 768 charcoal. Journal of Biobased Materials and Bioenergy, 6:69—74, 2012.
769 doi: 10.1166/jbmb.2012.1190.

770 [25] Wei Wang, Romain Lemaire, Ammar Bensakhria, and Denis Luart. Re771 view on the catalytic effects of alkali and alkaline earth metals (AAEMs) 772including sodium, potassium, calcium and magnesium on the pyrolysis 773 of lignocellulosic biomass and on the cc)-pyrolysis of coal with biomass. 774 Journal of Analytical and Applied Pyrolysis, 163: 105479, May 2022.
775 ISSN 0165-2370. doi: 10.1016/j.jaap.2022.105479.

776 [26] Sara Svensson. Minimizing the sulphur content in Kraft lignin. PhD 777 thesis, STFI-Packforsk, 2008.

778 [27] Sandip Kumar Singh, Subhrashis Banerjee, Kumar Vanka, and

779Paresh Laxmikant Dhepe. Understanding interactions between lignin 780 and ionic liquids with experimental and theoretical studies during cat781 alytic depolymerisation. Catalysis Today, 309:98—108, 7 2018. ISSN 782 0920-5861. doi: 10.1016/J.CATTOD.2017.09.050.

783 [28] Ayillath K. Deepa and Paresh L. Dhepe. Lignin depolymerization into 784 aromatic monomers over solid acid catalysts. ACS Catalysis, 5:365—379, 785 1 2015. ISSN 21555435. doi: 10.1021/CS501371Q.

786 [29] Sandip K. Singh, Anthony W. Savoy, Zhaoyang Yuan, Hao Luo, Shan787 non S. Stahl, Eric L. Hegg, and David B. Hodge. Integrated Two-Stage

788 Alkaline-Oxidative Pretreatment of Hybrid Poplar. Part 1: Impact of

789 Alkaline Pre-Extraction Conditions on Process Performance and Lignin 790 Properties. Industrial and Engineering Chemistry Research, 58(35):

791 15989-15999, sep 2019. ISSN 15205045. doi: 10.1021/acs.iecr.9b01124.

792 [30] Yo Rhin Rhim, Dajie Zhang, D. Howard Fairbrother, Kevin A. Wepas 793 nick, Kenneth J. Livi, Robert J. Bodnar, and Dennis C. Nagle. Changes 794 in electrical and microstructural properties of microcrystalline cellulose 795 as function of carbonization temperature. Carbon, 48: 1012—1024, 4 2010.

796 ISSN 00086223. doi: 10.1016/j.carbon.2009.11.020.

797 [31] A. Ferrari and J. Robertson. Interpretation of raman spectra of disor798 dered and amorphous carbon. Physical Review B - Condensed Matter 799 and Materials Physics, 61: 14095—14107, 2000. ISSN 1550235X. doi:

800 10.1103/PhysRevB.61.14095.

801 [32] Devin McGlamery, Alexander A. Baker, Yi-Sheng Liu, Martin A. Mos802 quera, and Nicholas P. Stadie. Phonon dispersion relation of bulk boron803 doped graphitic carbon. The Journal of Physical Chemistry C, 124(42):

804 23027-23037, 2020. doi: 10.1021/acs.jpcc.Oc06918.

805 [33] Seth Kane, Stephan Warnat, and Cecily Ryan. Improvements in meth
806 ods for measuring the volume conductivity of electrically conductive 807
carbon powders. Advanced Powder Technology, 32: 702—709, 3 2021.
808ISSN 0921-8831. doi: 10.1016/J.APT.2021.01.016.

809 [34] Abdul Awal and Mohini Sain. Spectroscopic studies and evaluation of glo
thermorheological properties of softwood and hardwood lignin. Journal 811 of
Applied Polymer Science, 122:956—963, 10 2011. ISSN 1097-4628. doi:
812 10.1002/APP.34211.
813 [35] E. Jakab, F. Till, T. Székely, and O. Faix. Thermogravimetry/mass 814
spectrometry of various lignosulfonates as well as of a kraft and aceto815
solv lignin. Holzforschung, 45:355—360, 1 1991. ISSN 1437434X. doi:
816 10.1515/HFSG.1991.45.5.355.

817 [36] Rhea J. Sammons, David P. Harper, Nicole Labbe, Joseph J. 818
Bozell, Thomas Elder, and Timothy G. Rials. Character819 ization of
organosolv lignins using thermal and ft-ir spec820troscopic analysis.
BioResources, 8:2752—2767, 2013. URL
821 https://bioresources.cnr.ncsu.edu/resources/characterization- of 822
organosolv- lignins- using- thermal- and- ft- ir- spectroscopic- analysis/.

823 [37] National Institute of Standards and Technology. Sodium sulfate, 2021.
824URL https://webbook.nist.gov/chemistry/.

825 [38] Santosh M. Bobade, P. Gopalan, and A. R. Kulkarni. Phase transition in 826
na2s04: All five polymorphic transformations in dsc. Ionics, 15:353—355, 8276 2009.
ISSN 09477047. doi: 10.1007/S11581-008-0272-6.

828 [39] Binod Shrestha, Yann Le Brech, Thierry Ghislain, Sébastien Leclerc,
829Vincent Carré, Frédéric Aubriet, Sandrine Hoppe, Philippe Marchal,

830Steve Pontvianne, Nicolas Brosse, and Anthony Dufour. A multitechgal nique characterization of lignin softening and pyrolysis. ACS Sustainable 832 Chemistry and Engineering, 5:6940—6949, 8 2017. ISSN 21680485. doi: 833 10.1021/ACSSUSCHEMENG.7B01130.

834 [40] M.M. Nassar and G.D.M. MacKay. Mechanism of thermal decomposi835tion of lignin. Wood and Fiber Science, 3, 1984.

836 [41] Ramesh K Sharma, Jan B Wooten, Vicki L Baliga, Xuehao Lin, W Ge837offrey Chan, and Mohammad R Hajaligol. Characterization of chars 838from pyrolysis of lignin. Fuel, 83(11):1469—1482, August 2004. ISSN 839 0016-2361. doi: 10.1016/j.fue1.2003.11.015.

840 [42] Yee Wen Chua, Hongwei Wu, and Yun Yu. Interactions between Low841and High-Molecular-Weight Portions of Lignin during Fast Pyrolysis at 842 Low Temperatures. Energy & Fuels, 33(11):11173—11180, November 843 2019. doi: 10.1021/acs.energyfuels.9b02813.

844 [43] Chenting Zhang, Yuewen Shao, Lijun Zhang, Shu Zhang, Roel J.M. 845 Westerhof, Qing Liu, Peng Jia, Qingyin Li, Yi Wang, and Xun Hu. 846 Impacts of temperature on evolution of char structure during pyrolysis 847 of lignin. Science of the Total Environment, 699: 134381, 1 2020. ISSN 848 18791026. doi: 10.1016/j.scitotenv.2019.134381.

849 [44] TW Samadhi, LE Jones, and AG Clare. Sox emissions from glass man850 ufacturing: Decomposition of sodium sulfate as influenced by carbon. 851 Glass Science And Technology-Glastechnische Berichte, 73(C2) :361–369g52 2000. ISSN 0946-7475.

853 [45] Hiromi Aso, Koichi Matsuoka, Atul Sharma, and Akira Tomita. Eval854 uation of size of graphene sheet in anthracite by a temperature855

programmed oxidation method. Energy and Fuels, 18: 1309—1314, 9 2004.

856 ISSN 08870624. doi: 10.1021/EF030176X.

857 [46] A. Celzard, J. F. Mareché, F. Payot, and G. Fürdin. Electrical conduc858 tivity of carbonaceous powders. Carbon, 40(15):2801—2815, jan 2002.

859 ISSN 00086223. doi:10.1016/S0008-6223(02)00196-3.

860 [47] SpectraBase. Sodium sulfate anhydrous. URL https:/[spectrabase.com/ 861 compound/9qW84EFMyGK#4WE3S08ipx8.

862 [48] John McDonald-Wharry. 2013—2014 survey of chars using raman spec863 troscopy. C 2021, Vol. 7, Page 63, 7:63, 8 2021. ISSN 2311-5629. doi:

864 10.3390/C7030063.

865 [49] E. R. Buiel, A. E. George, and J. R. Dahn. Model of micropore closure in 866 hard carbon prepared from sucrose. Carbon, 37(9):1399—1407, January 867 1999. doi: 10.1016/S0008-6223(98)00335-2.

868 [50] J. R. Dahn, W. Xing, and Y. Gao. The "falling cards model" for the 869 structure of microporous carbons. Carbon, 35(6):825—830, January 1997.

870ISSN 0008-6223. doi:10.1016/S0008-6223(97)00037-7.

871 [51] Rui Yu, Junxiang Xiang, Kaifa Du, Bowen Deng, Di Chen, Huayi Yin, 872 Ze Liu, and Dihua Wang. Electrochemical Growth of High-Strength 873 Carbon Nanocoils in Molten Carbonates. Nano Letters, 22(1):97—104,

874 January 2022. doi: 10.1021/acs.nanolett.1c03284.

875 [52] Maiyong Zhu, Yu Yang, and Yunping Ma. Salt-assisted synthesis of 876advanced carbon-based materials for energy-related applications.

Green Chemistry, 25(24):10263–10303, 2023. doi: 10.1039/D3GC03080F.

[53] Jong Chan Hyun, Hyeong Min Jin, Jin Hwan Kwak, Son Ha, Dong Hyuk Kang, Hyun Soo Kim, Sion Kim, Minhyuck Park, Chan Yeol Kim, Juhee Yoon, Ji Sung Park, Ji-Young Kim, Hee-Dae Lim, Se Youn Cho, Hyoung-Joon Jin, and Young Soo Yun. Design guidelines for a high-performance hard carbon anode in sodium ion batteries. Energy & Environmental Science, 17(8):2856—2863, April 2024. doi: 10.1039/D4EE00315B.

CRediT author statement

S.K.: conceptualization, methodology, validation, formal analysis, investigation, writing — original draft, writing — review & editing, visualization.

D.B.H.: methodology, writing — review & editing, supervision, funding acquisition

B. S.: methodology, investigation, writing — original draft

V.E.B.: methodology, investigation, writing — original draft

D.N.D.: methodology, investigation, writing — original draft

C. R.: methodology, writing — review & editing, supervision, project administration, funding acquisition

Declaration of interests

☒ The authors declare that they have no known competing financial interests or personal relationships that could have appeared to influence the work reported in this paper.

O The authors declare the following financial interests/personal relationships which may be considered as potential competing interests:

Electrical conductivity of lignin pyrolyzed at 1100 °c varies by a factor of 100

Na2S04 in lignin increases the size of graphitic crystallites, decreases conductivity

High aspect ratio graphitic crystallites are proposed as cause of this behavior Lignin-derived biochar carbon structure can be tuned by varying Na2S04 content